CHEMISTRY OF MATERIALS

Open Access

pubs.acs.org/cm

Article

$MnCaTa_2O_7$—A Magnetically Ordered Polar Phase Prepared via Cation Exchange

Subhadip Mallick, Fabio Orlandi, Pascal Manuel, Weiguo Zhang, P. Shiv Halasyamani, and Michael A. Hayward*

Cite This: *Chem. Mater.* 2023, 35, 7839–7846

Read Online

ACCESS | Metrics & More | Article Recommendations | Supporting Information

ABSTRACT: Reaction between the pseudo-Ruddlesden-Popper phase $Li_2CaTa_2O_7$ and $MnCl_2$ at 375 °C yields $MnCaTa_2O_7$, a paramagnetic polar phase (space group $P2_1nm$), which adopts an $a^-b^-c^+/b^-a^-c^+$ distorted, layered perovskite structure. Magnetization and neutron diffraction data show that $MnCaTa_2O_7$ adopts an antiferromagnetically ordered state below T_N = 56 K and exhibits large lattice parameter anomalies and a transient increase in its polar distortion mode at T_A = 50 K. However, in contrast to the related phase $MnSrTa_2O_7$, $MnCaTa_2O_7$ shows no strong signature of weak ferromagnetism and thus shows no signs of magnetoelectric coupling. The differences in physical behavior between the two $MnATa_2O_7$ phases appear to be related to their differing Mn cation-order and differing TaO_6 tilting schemes and demonstrate that even subtle changes to these orderings can have large effects on the distortion-mode couplings, which drive complex behavior of this class of "hybrid improper" ferroelectric material.

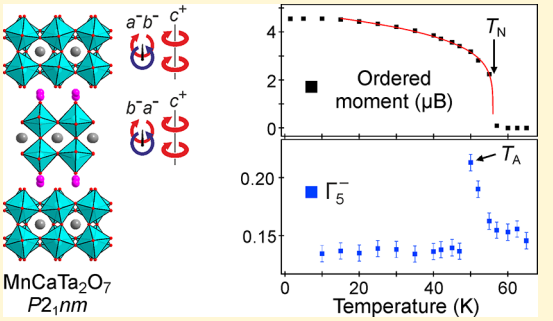

INTRODUCTION

Magnetoelectric multiferroic materials simultaneously exhibit a spontaneous, switchable electrical polarization (ferroelectricity) and a spontaneous, switchable magnetic polarization (ferromagnetism)[1,2] and are highly desired because they could allow the construction of novel devices with applications in digital data manipulation and storage.[3,4] However, the preparation of novel materials which display magnetoelectric behavior, is challenging. This is principally because materials can only exhibit ferroelectric behavior if they adopt noncentrosymmetric (NCS) crystal structures,[5,6] and unfortunately, asymmetric packing schemes tend to be thermodynamically disfavored compared to centrosymmetric alternatives, making ferroelectric behavior, and thus magnetoelectric behavior, rare.

Conventionally, ferroelectric behavior has been introduced into materials, by utilizing electronically driven structural distortions which break the inversion symmetry of a phase. Typically, these symmetry-breaking distortions are driven by a second-order Jahn-Teller (SOJT) instability[7] arising from the inclusion of either octahedrally coordinated d^0 transition-metal cations (e.g., Ti^{4+} in $BaTiO_3$)[8,9] or ns^2 posttransition-metal cations (e.g., Pb^{2+} in $PbZrO_3$),[10,11] which, in favorable circumstances, yield NCS crystal structures and induce polar behavior.

While the use of SOJT distortions has been successful in preparing a range of polar phases, the need to include d^0 and/or ns^2 cations limits the chemical diversity of polar materials and the "closed shell", diamagnetic electronic configurations of these ions disfavors magnetism.[12] Recently, an alternative "trilinear-coupled hybrid-improper" mechanism for stabilizing NCS structures has been receiving attention.[13] In this stabilization scheme, two nonpolar distortions (typically the low-energy octahedral tilting distortions of layered perovskites phases) couple together to stabilize a third polar distortion mode, which is unstable in the absence of the stabilizing nonpolar distortions. As the polar distortion mode is not the primary order parameter of the ferroelectric phase transition, materials of this type are often referred to as "hybrid improper" ferroelectrics.[13−15]

As noted above, in contrast to the SOJT stabilization of NCS phases, the trilinear-coupled hybrid-improper mechanism does not rely on the electronic features of a phase (i.e., d^0 or ns^2 ion configurations). Thus, in principle, it places no restrictions on the chemical composition of polar materials of this type, facilitating the inclusion of paramagnetic ions in polar materials. Indeed, one of the first materials predicted to exhibit trilinear-coupled ferroelectric behavior, $Ca_3Mn_2O_7$, adopts a weak ferromagnetic state at low temperature, which

Received: July 26, 2023
Revised: August 30, 2023
Published: September 9, 2023

https://doi.org/10.1021/acs.chemmater.3c01850
Chem. Mater. 2023, 35, 7839−7846

is observed to be magnetoelectrically coupled to the electrical polarization of the phase.[13]

However, further investigation of the layered Ruddlesden-Popper[16−21] and Dion-Jacobson[22−25] oxide phases, which exhibit hybrid improper ferroelectric behavior, reveals that this class of materials does not have as much "chemical freedom" as it may appear at first sight.[15] This is because the hybrid improper mechanism utilizes a coupling between two distinct octahedral tilting distortions. This requires phases with highly distorted structures that are only stable in layered perovskite materials with small Goldschmitt tolerance factors, estimated to be t <0.87.[15,17] Given that the tolerance factor, t, is defined as t = <A−O> / ($\sqrt{2}$ × <B−O>),[26] sufficiently distorted frameworks are only stable in compounds with small A-cations and large B-cations. This condition acts to exclude a large number of A/B cation combinations from exhibiting hybrid improper ferroelectric behavior, including the majority of preparable Ruddlesden-Popper and Dion-Jacobson oxides with paramagnetic cations on the B-site.[15]

To address this limitation, we have been using the facile cation-exchange chemistry of $A'AB_2O_7$ Dion-Jacobson[27−29] and $Li_2AB_2O_7$ pseudo-Ruddlesden-Popper oxides[30] to prepare metastable layered perovskite phases with small tolerance factors, to investigate the possibility of trilinear-coupled hybrid-improper ferroelectric behavior in these materials. Building on this work, we have demonstrated that paramagnetic Mn^{2+} cations can be exchanged for Li^+ ions in the pseudo-Ruddlesden-Popper oxide $Li_2SrTa_2O_7$, to yield $MnSrTa_2O_7$, a paramagnetic polar phase that exhibits signatures of magnetoelectric coupling at low temperature.[31] Here, we describe a study of the related phase, $MnCaTa_2O_7$, prepared via an analogous cation-exchange reaction from $Li_2CaTa_2O_7$.

EXPERIMENTAL SECTION

Synthesis of $Li_2CaTa_2O_7$. Polycrystalline samples of $Li_2CaTa_2O_7$ were prepared by a ceramic synthesis method from Ta_2O_5 (99.9985%, dried at 900 °C), $CaCO_3$ (99.8%), and Li_2CO_3 (99.998%). Suitable stoichiometric ratios of Ta_2O_5 and $CaCO_3$ were ground together in an agate pestle and mortar and combined with a 3% excess of Li_2CO_3 (to compensate for loss due to volatilization at high temperature). These mixtures were placed in an alumina crucible and heated at 800 °C in the air for 12 h. The mixtures were then reground, pressed into 13 mm pellets, and heated at 1200 °C for two periods of 2 h. The samples were reground between heating cycles, pressed into pellets, placed in an alumina crucible, and directly put in a furnace, which was kept at 1200 °C.

Preparation of $MnCaTa_2O_7$. $MnCaTa_2O_7$ was prepared via a cation exchange reaction from $Li_2CaTa_2O_7$. $Li_2CaTa_2O_7$ was ground together with anhydrous $MnCl_2$ in a 1:5 molar ratio using an agate pestle and mortar in an argon-filled glove box. The mixture was then heated at 375 °C for 3 days under flowing argon. The reaction mixture was then washed with distilled water to remove the remaining chlorides.

Magnetization data, described below, showed that samples of $MnCaTa_2O_7$ contained small quantities of Mn_3O_4 (a ferrimagnet, T_N ~43 K[32,33]) not detectable by diffraction. To remove this magnetic impurity, a sample was heated to 350 °C under a flow of 10% H_2 in argon, to reduce the Mn_3O_4 to MnO. SXRD data collected after this reduction process showed no changes with respect to the initial material.

Characterization. X-Ray powder diffraction data were collected using a PANalytical X'pert diffractometer incorporating an X'celerator position-sensitive detector (monochromatic Cu Kα_1 radiation). High-resolution synchrotron X-ray powder diffraction (SXRD) data were collected using the I11 instrument at the Diamond Light Source Ltd. Diffraction patterns were collected using Si-calibrated X-rays with an approximate wavelength of 0.825 Å from samples, sealed in 0.3 mm diameter borosilicate glass capillaries. Time-of-flight neutron powder diffraction (NPD) data were collected using the GEM diffractometer (ambient temperature) and WISH diffractometer[34] (low temperature) located at the ISIS neutron source, from the samples loaded in vanadium cans. Rietveld refinements were performed using the TOPAS Academic (V6) package.[35] Second harmonic generation (SHG) response of samples was measured from powder samples with the SHG intensity compared to a standard sample of α-SiO_2. No index matching fluid was used in any of the experiments. A detailed description of the experimental setup and process has been reported previously.[36] DC magnetization data were collected using a Quantum Design MPMS SQUID magnetometer from samples contained in gelatin capsules.

RESULTS

Structural Characterization of $Li_2CaTa_2O_7$. SXRD data collected from $Li_2CaTa_2O_7$ could be indexed by an orthorhombic unit cell (a = 5.51225(3) Å, b = 5.46373(3) Å, c = 18.2321(1) Å) with reflection conditions consistent with the $Pna2_1$ (#33) space group previously reported for the phase.[37,38] Thus, a model based on the previously reported structure of $Li_2CaTa_2O_7$ was refined against the SXRD data to achieve a good fit (wRp = 1.32%; R_{Bragg} = 1.43%) yielding a structural model in good agreement with previous reports,[37] as described in detail in the Supporting Information.

Structural Characterization of $MnCaTa_2O_7$. SXRD and NPD data (GEM) collected from the manganese exchanged sample of $Li_2CaTa_2O_7$, henceforth referred to as $MnCaTa_2O_7$, could be indexed using a primitive orthorhombic unit cell (a = 5.5155(4) Å, b = 5.5169(4) Å, c = 19.0303(12) Å) consistent with a $\sqrt{2} \times \sqrt{2} \times 1$ geometric expansion of an aristotype n = 2 Ruddlesden-Popper framework. Powder SHG measurements reveal that $MnCaTa_2O_7$ is SHG active (0.45 times α-SiO_2), indicating the phase adopts a noncentrosymmetric crystal structure. A symmetry analysis of the structural tilting distortions of n = 2 Ruddlesden-Popper phases[27,39] revealed two candidate noncentrosymmetric structures with space group symmetries consistent with the reflection conditions observed in the diffraction data: $P2_1nm$ (#31) and $P2cm$ (#28), which exhibit $a^-b^-c^+/b^-a^-c^+$ and $a^-b^-c^+/-(a^-b^-)c^+$ tilting distortions, respectively. Structural models were constructed to describe these two distorted frameworks and refined against the diffraction data.

There are two crystallographically distinct interlayer tetrahedral coordination sites in both the $P2_1nm$ and $P2cm$ symmetry models, allowing both Mn site-ordered and site-disordered structures to be described by both the $P2_1nm$ and $P2cm$ models. Initially, in refinements against PND data, the manganese cations were distributed across both sites to describe site-disordered Mn cation arrangements in both models. However, refinement of the Mn site occupancies led to the majority of the Mn cations (>98%) being located on one of the sites in the $P2_1nm$ symmetry model, accompanied by a large improvement in the fit to the data. Thus, a Mn cation-ordered model was adopted for the $P2_1nm$ symmetry model. In contrast, the $P2cm$ symmetry model retained a Mn site-disordered arrangement when the Mn site occupancies were refined. The difference in refined Mn site-order between the $P2_1nm$ and $P2cm$ symmetry models can be rationalized by observing that the two crystallographically distinct Mn sites in the $P2_1nm$ symmetry model are arranged as a chequerboard,

https://doi.org/10.1021/acs.chemmater.3c01850
Chem. Mater. 2023, 35, 7839−7846

while the analogous sites in the *P2cm* symmetry model are arranged in stripes.

On convergence, it was clear that the $P2_1nm$ symmetry model gave a much better fit to the NPD data (wRp = 2.87%, Rp = 3.08%) compared to the *P2cm* symmetry model (wRp = 8.58%, Rp = 5.75%), indicating that the structure of $MnCaTa_2O_7$ is best described by the $P2_1nm$ symmetry model. On convergence, the Mn site occupancy refined to 1.01(1) on the majority site and −0.01(2) on the minority site, so these were set to unity and zero, respectively, consistent with the $MnCaTa_2O_7$ composition. The NPD data showed no evidence for any other phases in the sample. Plots of the fitted NPD data are shown in Figure 1, with full details of the refined

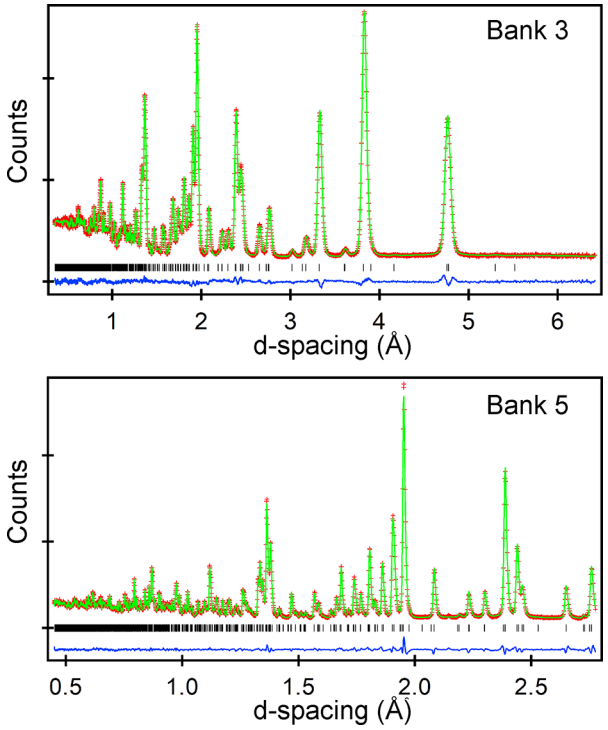

Figure 1. Observed, calculated, and difference plots from the structural refinement of $MnCaTa_2O_7$ against NPD data (GEM) collected at room temperature. Data from detector banks 3 (2θ = 35°) and 5 (2θ = 91°) are shown. Data from all detector banks are shown in the Supporting Information.

structure of $MnCaTa_2O_7$ are given in the Supporting Information. A representation of the refined structure is shown in Figure 2. It should be noted that, while the tilting distortion of $MnCaTa_2O_7$ is $a^-b^-c^+/b^-a^-c^+$, it is close to $a^-b^0c^+/b^0a^-c^+$ as the "*a*" tilt (19.7(1)°) is significantly larger than the "*b*" tilt (1.1(1)°).

Magnetic Characterization of $MnCaTa_2O_7$. Zero-field-cooled (ZFC) and field-cooled (FC) magnetization data were collected from a sample of H_2-treated $MnCaTa_2O_7$ in an applied field of 100 Oe (Figure 3). These data can be fit by the Curie−Weiss law in the range 165 < *T*/K < 300 to yield values of C = 5.829(4) cm^3 K mol^{-1} and θ = −180.0(3) K, as shown in detail in the Supporting Information. The extracted Curie constant is slightly larger than that expected for an array of S = 5/2 Mn^{2+} centers ($C_{expected}$ = 4.37 cm^3 K mol^{-1}). On cooling below T ~150 K, the magnetization data exhibit a broad local maximum before the ZFC and FC data diverge below T ~100 K, with the divergence increasing significantly below T ~45 K.

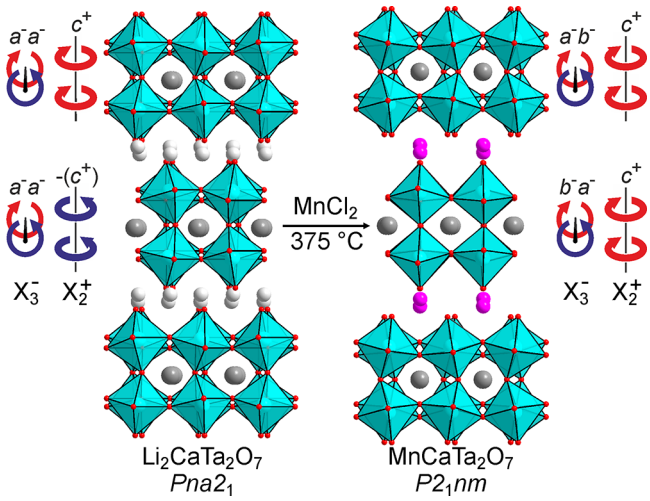

Figure 2. Crystal structures of $Li_2CaTa_2O_7$ and $MnCaTa_2O_7$. Light gray, dark gray, purple, blue and red spheres represent Li, Ca, Mn, Ta, and O, respectively. Arrows indicate octahedral tilting schemes.

Magnetization-field data collected at 300 K are linear and pass through the origin, as shown in Figure 3, while analogous data collected at 5 K, after cooling in an applied field of 50,000 Oe, are slightly sigmoidal but exhibit no significant hysteresis.

NPD data (WISH) collected at 1.5 K from $MnCaTa_2O_7$ exhibit a series of diffraction peaks, not observed in the analogous data collected at room temperature (Figure 4b), which are attributed to a magnetic ordering of the manganese spins. The additional diffraction peaks could be indexed using a single magnetic propagation vector, $\boldsymbol{k}$ = (0, 0, 0), of the crystallographic unit cell. The structural model (space group $P2_1nm$) was used to generate possible magnetic models, with the help of the ISODISTORT software package,[40,41] which were refined against the 1.5 K neutron data. The best fit to the data was achieved using a model in magnetic space group $P2_1n'm'$, in which Mn spins are aligned parallel to the *z*-axis and adopt a G-type antiferromagnetic ordered arrangement. Refinement of the components of the Mn moments revealed that the magnitude of the ordered moment along *x*- and *y*-directions is zero within error. Therefore, the model was simplified to only allow an ordered moment along the *z*-direction (as shown in Figure 4a), which refined to a value of 4.496(8) μB. Full details of the crystal and magnetic structure are given in the Supporting Information along with the fit to the NPD data.

NPD data (WISH) collected on warming from 1.5 K reveal a decline in the ordered magnetic moment with increasing temperature, which can be fit by a power law ($M = M_0(1 - T/T_N)^{\beta}$), as shown in Figure 4c, to yield values of M_0 = 4.85(3) μB, T_N = 55.9(1) K, β = 0.192(7). Close inspection of the NPD data sets (Figure 4b) reveals that magnetic scattering persists above T_N (56 K) with the magnetic scattering features broadening significantly with increasing temperature, as shown in detail in the Supporting Information.

DISCUSSION

Treatment of $Li_2CaTa_2O_7$ with $MnCl_2$ leads to a quantitative, topochemical, Mn-for-Li cation exchange of the host phase resulting in the formation of phase pure $MnCaTa_2O_7$. Diffraction and SHG data reveal that $MnCaTa_2O_7$ adopts a distorted n = 2 Ruddlesden-Popper structure, described in the

https://doi.org/10.1021/acs.chemmater.3c01850
Chem. Mater. 2023, 35, 7839−7846

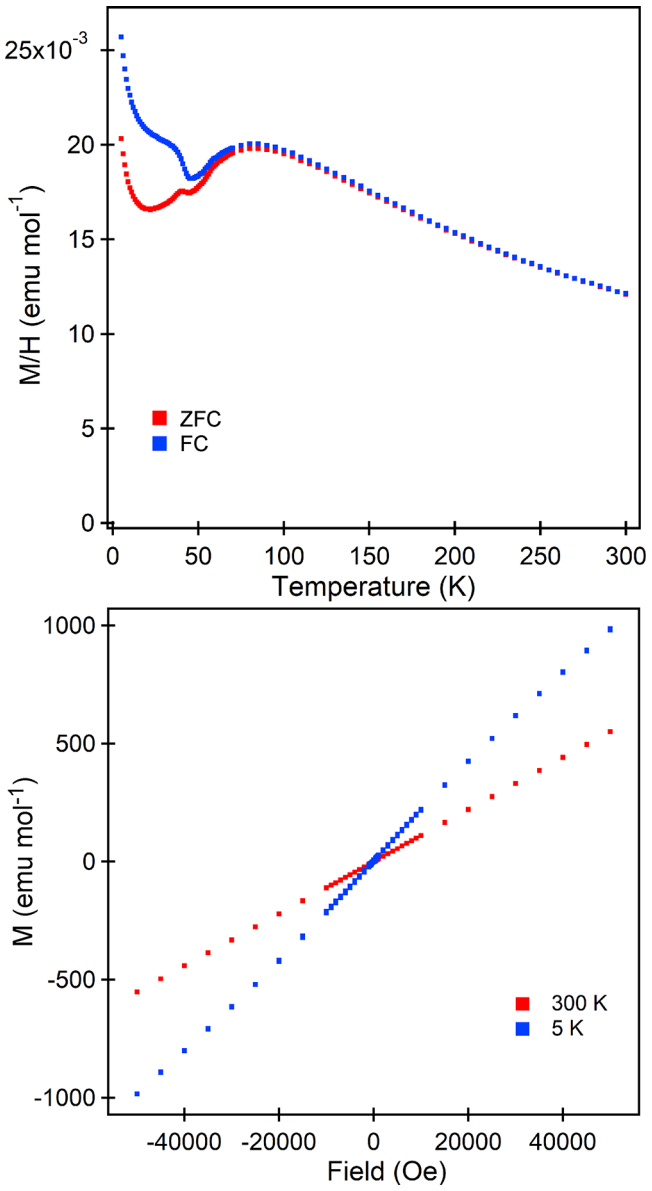

Figure 3. (top) Zero-field-cooled and field-cooled magnetization data collected from $MnSrTa_2O_7$ as a function of temperature in an applied field of 100 Oe. (bottom) Magnetization-field data collected from $MnCaTa_2O_7$ at 300 and 5 K.

polar space group $P2_1nm$. This distorted structure can be related to an Mn-disordered, undistorted aristotype phase (space group $I4/mmm$) by the application of a series of symmetry-lowering distortions with symmetries described by the irreducible representations (irreps) of the parent $I4/mmm$ space group. Initially, the ordering of the Mn cations into a chequerboard arrangement lowers the symmetry of the phase (and expands the unit cell) consistent with the M_2^+ irrep. Subsequently, there are 7 displacive distortions, which are symmetry-allowed on descent from $I4/mmm$ to $P2_1nm$ space group symmetry: Γ_1^+, Γ_5^-, X_1^+, $X_2^+(0;a)$, $X_3^-(b;c)$, M_2^+, and M_5^-. However, analysis of the room-temperature structure of $MnCaTa_2O_7$ reveals that only 3 of these allowed displacive distortion modes have significant magnitude: $X_3^-(b;c)$, which principally describes the $a^-b^-c^0/b^-a^-c^0$ tilting distortion; $X_2^+(0;a)$, which principally describes the $a^0a^0c^+/a^0a^0c^+$ tilting distortion; and Γ_5^-, which describes a polar cation displacement. The symmetries of these distortion modes are consistent with the trilinear-coupling polar stabilization mechanism, in which the $X_3^-(b;c)$ and $X_2^+(0;a)$ distortions couple to and stabilize the Γ_5^- polar distortion, as seen in a range of other layered perovskite phases.[15]

It is interesting to note that the parent phase, $Li_2CaTa_2O_7$, also adopts a polar structure, described in space group $Pna2_1$, related to the $I4/mmm$ aristotype structure via the application of an $X_3^-(b;0)$ $a^-a^-c^0/a^-a^-c^0$ tilt, an $X_2^+(0;a)$ $a^0a^0c^+/a^0a^0{-}c^+$ tilt and a Γ_3^- polar distortion.[37,38] However, in this instance, the polar distortion is not stabilized via trilinear coupling to the $X_3^-(b;0)$ and $X_2^+(0;a)$ tilts but via an SOJT stabilization mechanism via the TaO_6 units, as demonstrated by the observation of a phase transition at T ~490 K to a nonpolar phase, described in space group $Pnam$, which retains the $X_3^-(b;0)$ and $X_2^+(0;a)$ distortions but not the polar distortion.[37] Thus, the substitution of Li by Mn retains a noncentrosymmetric framework but changes the mechanism by which polarization is stabilized, suggesting that these two stabilization mechanisms operate on similar energy scales, as observed previously in other layered perovskite systems.[30]

A further comparison can be made between $MnCaTa_2O_7$ and $MnSrTa_2O_7$. Both phases share a common aristotype structure, but in contrast to $MnCaTa_2O_7$, $MnSrTa_2O_7$ adopts a polar structure described in space group $A2_1am$ related to the aristotype phase via $X_3^-(0;c)$ $a^-a^-c^0/a^-a^-c^0$ and $X_2^+(0;a)$ $a^0a^0c^+/a^0a^0c^+$ tilts and a Γ_5^- polar distortion, with the symmetries of these distortions again compatible with a trilinear-coupled stabilization mechanism.[31] A further difference between the Ca and Sr phases is that the Mn cations in $MnSrTa_2O_7$ exhibit an incommensurately modulated ordering (Y_2 symmetry), which can be locally described as a chequerboard arrangement, but which inverts filled and vacant positions with a period, which is incommensurate with the underlying $SrTa_2O_7$ framework, in contrast to the long-range commensurate chequerboard order of the Mn cations in $MnCaTa_2O_7$.[31]

The differing octahedral tilts and Mn cation orderings observed for $MnCaTa_2O_7$ and $MnSrTa_2O_7$ can be rationalized by noting that, although chequerboard ordering appears to be the optimum arrangement for minimizing Mn-Mn cation repulsion, the commensurate chequerboard ordering exhibited by $MnCaTa_2O_7$ is not symmetry compatible with the $a^-a^-c^+/a^-a^-c^+$ distorted, $A2_1am$ symmetry framework exhibited by $MnSrTa_2O_7$ as all the pseudo-tetrahedral Mn coordination sites are symmetry equivalent in the $A2_1am$ space group. More formally, we can note that the M_2^+ irrep, which describes the symmetry lowering due to the chequerboard ordering of Mn cations, is not allowed to have a nonzero magnitude on the descent in symmetry from $I4/mmm$ to $A2_1am$. Thus, there appears to be a conflict between the optimum octahedral tilting arrangement ($a^-a^-c^+/a^-a^-c^+$) and the optimum Mn cation ordering (M_2^+ chequerboard ordering), with the octahedral tilting "winning" the competition in $MnSrTa_2O_7$ ($a^-a^-c^+/a^-a^-c^+$ tilt, incommensurate Mn order) and the chequerboard Mn ordering "winning" in $MnCaTa_2O_7$ ($a^-b^-c^+/b^-a^-c^+$ tilt, chequerboard Mn order), illustrating again that there are a large number of competing ground states in these layered perovskite phases.

The subtle structural differences between $MnCaTa_2O_7$ and $MnSrTa_2O_7$ lead to differences in their physical behavior. As noted previously, on cooling $MnSrTa_2O_7$ adopts G-type antiferromagnetic order (T_N = 43 K) and on further cooling

https://doi.org/10.1021/acs.chemmater.3c01850
Chem. Mater. 2023, 35, 7839−7846

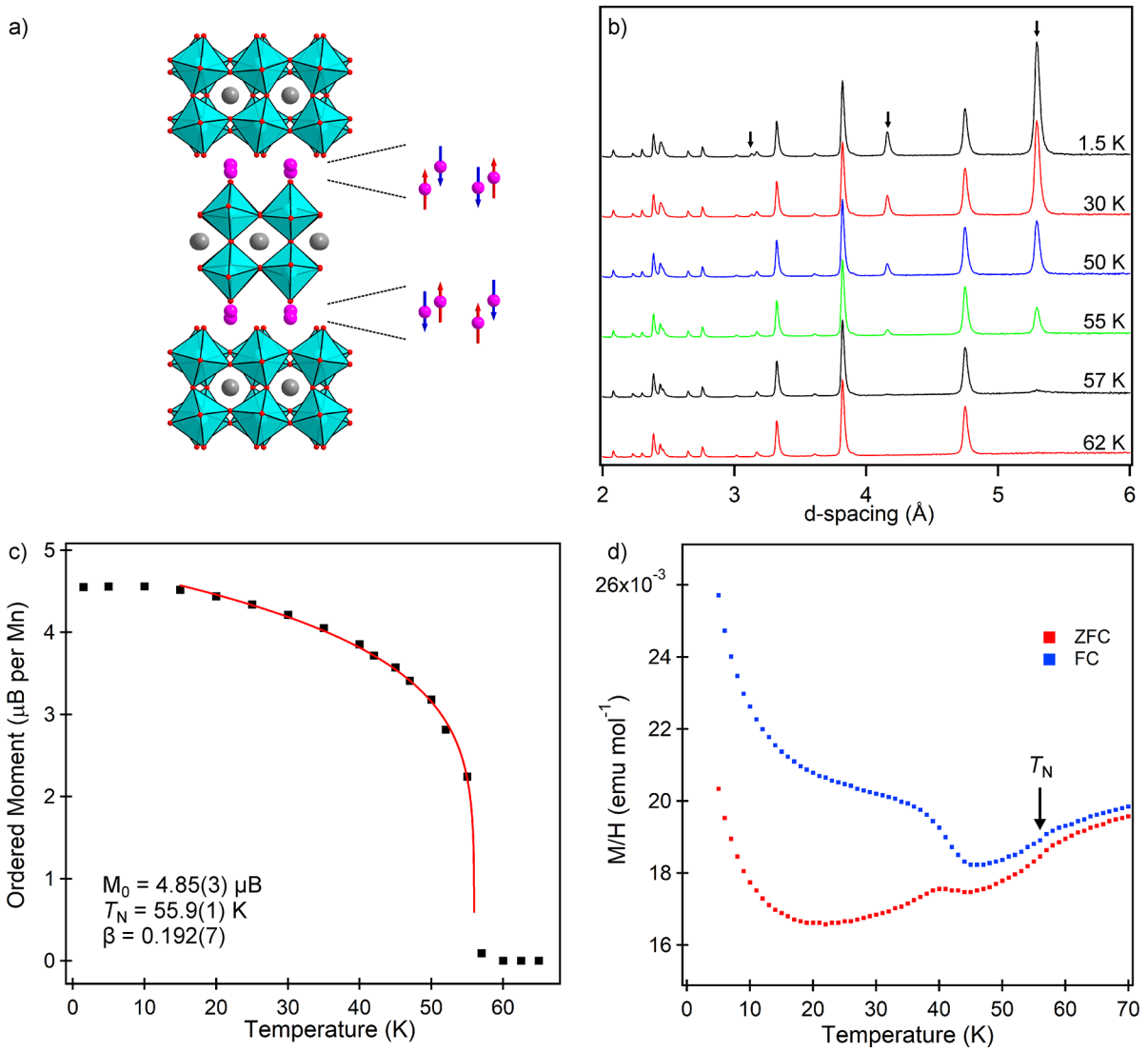

Figure 4. (a) G-type magnetic structure of $MnCaTa_2O_7$. (b) NPD data collected from $MnCaTa_2O_7$ as a function of temperature. Arrows indicate magnetic diffraction peaks. (c) Plot of ordered magnetic moment as a function of temperature, fitted by $(M = M_0(1 - T / T_N)^{\beta}$ power law. (d) ZFC and FC magnetization data from $MnCaTa_2O_7$ in range $5 < T/K < 70$.

to T_A = 38 K, local minima are observed in the *a* and *c* lattice parameters, and discontinuities are observed in the magnitudes of the $X_3^-(0;c)$ and Γ_5^- distortion modes, accompanied by a large increase in the ferromagnetic component of the magnetic order of the material. The simultaneous change in the magnitudes of both the electrical and magnetic polarizations is taken as a signature of magnetoelectric coupling.[31]

A similar analysis of $MnCaTa_2O_7$ using the NPD data (WISH) collected as a function of temperature reveals a shallow local minimum in the *a* lattice parameter at T = 55 K (i.e., T_N as determined from the magnetic scattering in the NPD data) and a deeper local minimum in the *b* and *c* lattice parameters at T_A = 50 K, as shown in Figure 5. Deconvoluting the refined structures of $MnCaTa_2O_7$ determined from these NPD data to extract the magnitudes of the distortion modes reveals that the variation in the $X_2^+(0;a)$ mode appears to track the variation in the *b* and/or *c* lattice parameters (Figure 5), while the magnitude of the $X_3^-(b;c)$ mode declines monotonically from T_N to T_A. In contrast, the Γ_5^- mode increases in magnitude by ~25% on cooling from T_N to T_A, before sharply returning to its original value below T_A. As shown in Figure 5, there are no dramatic changes in the magnetization data collected from $MnCaTa_2O_7$ at either T_N or T_A, with no sign of a large increase in the ferromagnetic component of the magnetic moment at T_A seen for $MnSrTa_2O_7$. Thus, we can conclude that there is no evidence for magnetoelectric coupling in $MnCaTa_2O_7$. The increase in the divergence between the ZFC and FC data seen below T ~40 K is attributed to an impurity phase in the sample, likely Mn_3O_4, which cannot be observed by diffraction.

The differing structural and magnetic behavior of $MnCaTa_2O_7$ and $MnSrTa_2O_7$ around their respective magnetic ordering temperatures is surprisingly given the apparent similarity of the phases. Both derive from identical $MnATa_2O_7$ aristotype parent structures, both adopt polar structural distortions with the polarization aligned parallel to the *x*-axis, both adopt magnetic order with structures described in magnetic space groups, which allow net ferromagnetic moments aligned parallel to the *x*-axis, yet the magnetic and electric polarizations appear to couple in $MnSrTa_2O_7$ and not in $MnCaTa_2O_7$. The implication is that the differences in

https://doi.org/10.1021/acs.chemmater.3c01850
Chem. Mater. 2023, 35, 7839−7846

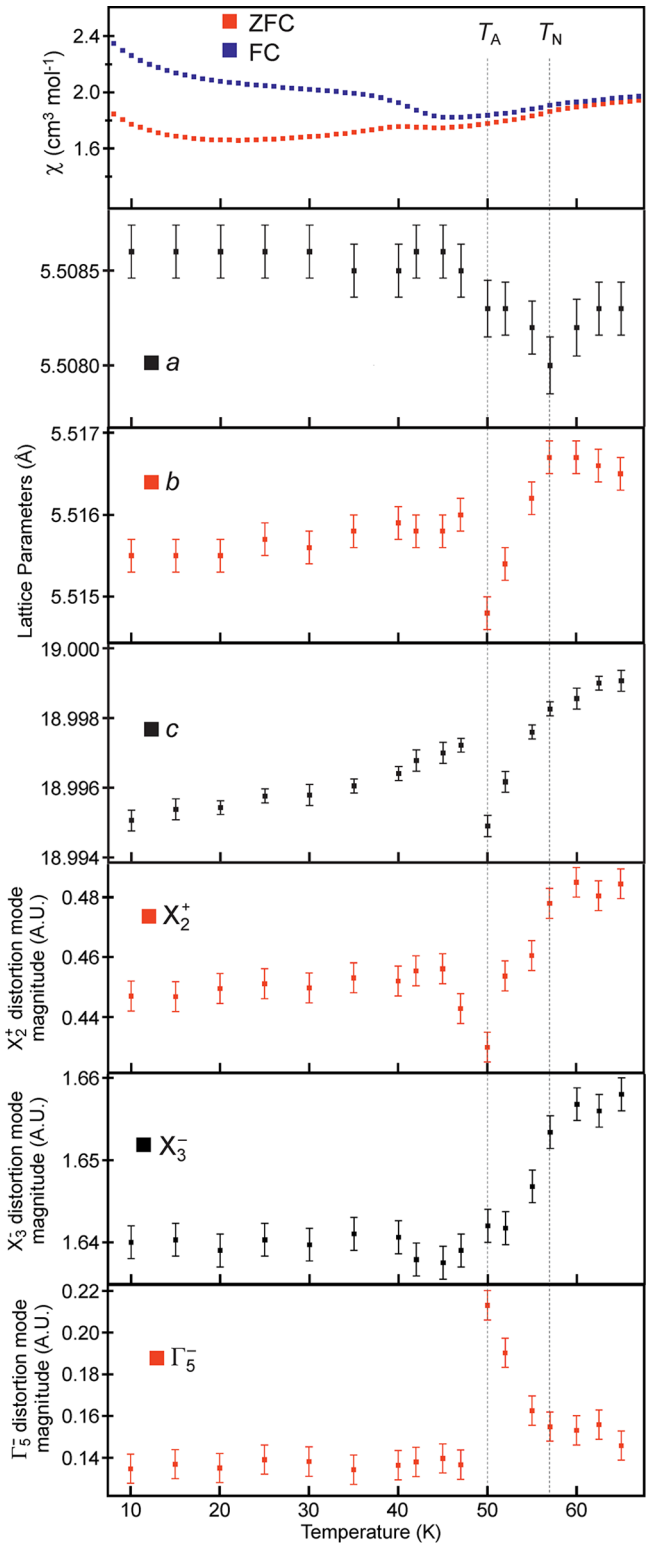

Figure 5. Zero-field cooled and field cooled magnetization data, lattice parameters, $X_2^+(0;a)$, $X_3^-(b;c)$ and Γ_5^- distortion mode magnitudes (arbitrary units) plotted as a function of temperature.

physical behavior arise from the subtle differences between the two phases.

The most obvious difference between the two phases is the combination of Mn cation-order and octahedral tilting distortion each exhibits: M_2^+ chequerboard Mn-order and an $X_3^-(b;c)$ $a^-b^-c^0/b^-a^-c^0$ tilt for $MnCaTa_2O_7$ compared to Y_2 incommensurate Mn-order and an $X_3^-(0;c)$ $a^-a^-c^0/a^-a^-c^0$ tilting distortion for $MnSrTa_2O_7$. However, these features of the materials do not appear to be immediately relevant to the appearance of a ferromagnetic polarization as our previous symmetry analysis of the magnetoelectric coupling in $MnSrTa_2O_7$ revealed that it is coupling between the $X_2^+(0;a)$ $a^0a^0c^+/a^0a^0c^+$ tilt and the mM_3^+ G-type magnetic order, which generates and stabilizes the $m\Gamma_5^+$ ferromagnetic polarization of the phase.[31]

However, given that both $MnSrTa_2O_7$ and $MnCaTa_2O_7$ exhibit $X_2^+(0;a)$ tilts and mM_3^+ magnetic order in their ground states, but only $MnSrTa_2O_7$ exhibits a significant ferromagnetic polarization, we can conclude that, while symmetry allowed, the coupling between $X_2^+(0;a)$ and mM_3^+ modes in $MnCaTa_2O_7$ is much weaker than in $MnSrTa_2O_7$. The origin of the weak $X_2^+(0;a)/mM_3^+$ coupling in $MnCaTa_2O_7$ is not clear. It does not appear to be due to the small magnitude of the $X_2^+(0;a)$ tilt in the calcium phase (~ 2.5 °), as the corresponding tilt in the strontium phase is also small (~1.5 °). Clearly, this issue warrants further attention and further highlights the complexities of the distortion mode couplings in this class of material.

CONCLUSIONS

Reaction between $Li_2CaTa_2O_7$ and $MnCl_2$ allows the preparation of the metastable phase $MnCaTa_2O_7$. Detailed structural characterization reveals $MnCaTa_2O_7$ adopts a layered perovskite structure in which the $CaTa_2O_7$ layers adopt an $a^-b^-c^+/b^-a^-c^+$ tilting distortion with the Mn^{2+} cations ordered in a chequerboard manner in the interlayer region. SHG data confirm that a noncentrosymmetric structure is adopted by $MnCaTa_2O_7$, which NPD data reveal is described in the space group $P2_1nm$. Symmetry analysis shows the experimental structure can be related to an undistorted aristotype structure (space group $I4/mmm$) via two tilting distortion modes $X_3^-(b;c)$, which principally describes the $a^-b^-c^0/b^-a^-c^0$ tilting distortion and $X_2^+(0;a)$, which principally describes the $a^0a^0c^+/a^0a^0c^+$ tilting distortion. These two tilting distortions appear to stabilize a polar Γ_5^- distortion via the trilinear-coupled hybrid improper stabilization mechanism. On cooling, $MnCaTa_2O_7$ adopts a G-type antiferromagnetically ordered structure below T_N = 56 K and exhibits large lattice parameter anomalies, especially in the b and c lattice parameters, at T_A = 50 K. However, in contrast to $MnSrTa_2O_7$, there is no change to the magnetization at T_A and no evidence for weak ferromagnetism in $MnCaTa_2O_7$ at any temperature.

ASSOCIATED CONTENT

Supporting Information

The Supporting Information is available free of charge at https://pubs.acs.org/doi/10.1021/acs.chemmater.3c01850.

Detailed description of the structural characterization of $Li_2CaTa_2O_7$ and $MnCaTa_2O_7$ at room temperature, and structural and magnetic characterization of $MnCaTa_2O_7$ at low temperature (PDF)

AUTHOR INFORMATION

Corresponding Author

Michael A. Hayward − *Department of Chemistry, Inorganic Chemistry Laboratory, University of Oxford, Oxford OX1 3QR, UK;* orcid.org/0000-0002-6248-2063; Email: michael.hayward@chem.ox.ac.uk

https://doi.org/10.1021/acs.chemmater.3c01850
Chem. Mater. 2023, 35, 7839−7846

Authors

Subhadip Mallick − *Department of Chemistry, Inorganic Chemistry Laboratory, University of Oxford, Oxford OX1 3QR, UK*

Fabio Orlandi − *ISIS Facility, Rutherford Appleton Laboratory, Oxon OX11 0QX, UK;* orcid.org/0000-0001-6333-521X

Pascal Manuel − *ISIS Facility, Rutherford Appleton Laboratory, Oxon OX11 0QX, UK*

Weiguo Zhang − *Department of Chemistry, University of Houston, Houston, Texas 77204-5003, United States*

P. Shiv Halasyamani − *Department of Chemistry, University of Houston, Houston, Texas 77204-5003, United States;* orcid.org/0000-0003-1787-1040

Complete contact information is available at: https://pubs.acs.org/10.1021/acs.chemmater.3c01850

Author Contributions

The manuscript was written through contributions of all authors.

Notes

The authors declare no competing financial interest.

■ ACKNOWLEDGMENTS

Experiments at the Diamond Light Source were performed as part of the Block Allocation Group award "Oxford/Warwick Solid State Chemistry BAG to probe composition-structure−property relationships in solids" (CY25166). Experiments at the ISIS pulsed neutron facility were supported by a beam time allocation from the STFC (doi.org/10.5286/ISIS.E.RB1910150-1). S.M. thanks Somerville College for an Oxford Ryniker Lloyd scholarship. P.S.H. and W.Z. thank the National Science Foundation (DMR-2002319) and Welch Foundation (Grant E-1457) for support.

■ REFERENCES

(1) Eerenstein, W.; Mathur, N. D.; Scott, J. F. Multiferroic and magnetoelectric materials. *Nature* **2006**, *442*, 759.

(2) Cheong, S. W.; Mostovoy, M. Multiferroics: a magnetic twist for ferroelectricity. *Nat. Mater.* **2007**, *6*, 13−20.

(3) Bibes, M.; Barthélémy, A. Multiferroics: Towards a magnetoelectric memory. *Nat. Mater.* **2008**, *7*, 425−426.

(4) Scott, J. F. Data storage: Multiferroic memories. *Nat. Mater.* **2007**, *6*, 256−257.

(5) Nye, F. J. *Physical Properties of Crystals*; Oxford University Press: Oxford, UK, 1957.

(6) Shiv Halasyamani, P.; Poeppelmeier, K. R. Noncentrosymmetric oxides. *Chem. Mater.* **1998**, *10*, 2753−2769.

(7) Pearson, R. G. The second-Order Jahn-Teller Effect. *J. Mol. Struct.* **1983**, *103*, 25−34.

(8) Cohen, R. E. Origin of Ferroelectricity in Perovskite Oxides. *Nature* **1992**, *358*, 136−138.

(9) Kunz, M.; Brown, I. D. Out-of-Center Distortions around Octahedrally Coordinated d^0 Transition-Metals. *J. Solid State Chem.* **1995**, *115*, 395−406.

(10) Seshadri, R.; Hill, N. A. Visualizing the Role of Bi 6s "Lone Pairs" in the Off-Center Distortion in Ferromagnetic $BiMnO_3$. *Chem. Mater.* **2001**, *13*, 2892−2899.

(11) Stoltzfus, M. W.; Woodward, P. M.; Seshadri, R.; Klepeis, J. H.; Bursten, B. Structure and Bonding in $SnWO_4$, $PbWO_4$, and $BiVO_4$: Lone Pairs vs Inert Pairs. *Inorg. Chem.* **2007**, *46*, 3839−3850.

(12) Hill, N. A. Why Are There So Few Magnetic Ferroelectrics? *J. Phys. Chem. B* **2000**, *104*, 6694−6709.

(13) Benedek, N. A.; Fennie, C. J. Hybrid Improper Ferroelectricity: A Mechanism for Controllable Polarization-Magnetization Coupling. *Phys. Rev. Lett.* **2011**, *106*, No. 107204.

(14) Benedek, N. A. Origin of Ferroelectricity in a Family of Polar Oxides: The Dion-Jacobson Phases. *Inorg. Chem.* **2014**, *53*, 3769−3777.

(15) Benedek, N. A.; Hayward, M. A. Hybrid Improper Ferroelectricity: A Theoretical, Computational, and Synthetic Perspective. *Annu. Rev. Mater. Res.* **2022**, *52*, 331−355.

(16) Oh, Y. S.; Luo, X.; Huang, F. T.; Wang, Y. Z.; Cheong, S. W. Experimental demonstration of hybrid improper ferroelectricity and the presence of abundant charged walls in $(Ca,Sr)_3Ti_2O_7$ crystals. *Nat. Mater.* **2015**, *14*, 407−413.

(17) Yoshida, S.; Akamatsu, H.; Tsuji, R.; Hernandez, O.; Padmanabhan, H.; Sen Gupta, A.; Gibbs, A. S.; Mibu, K.; Murai, S.; Rondinelli, J. M.; Gopalan, V.; Tanaka, K.; Fujita, K. Hybrid Improper Ferroelectricity in $(Sr,Ca)_3Sn_2O_7$ and Beyond: Universal Relationship between Ferroelectric Transition Temperature and Tolerance Factor in n = 2 Ruddlesden-Popper Phases. *J. Am. Chem. Soc.* **2018**, *140*, 15690−15700.

(18) Yoshida, S.; Fujita, K.; Akamatsu, H.; Hernandez, O.; Sen Gupta, A.; Brown, F. G.; Padmanabhan, H.; Gibbs, A. S.; Kuge, T.; Tsuji, R.; Murai, S.; Rondinelli, J. M.; Gopalan, V.; Tanaka, K. Ferroelectric $Sr_3Zr_2O_7$: Competition between Hybrid Improper Ferroelectric and Antiferroelectric Mechanisms. *Adv. Funct. Mater.* **2018**, *28*, 1801856.

(19) Liu, M.; Zhang, Y.; Lin, L.-F.; Lin, L.; Yang, S.; Li, X.; Wang, Y.; Li, S.; Yan, Z.; Wang, X.; Li, X.-G.; Dong, S.; Liu, J.-M. Direct observation of ferroelectricity in $Ca_3Mn_2O_7$ and its prominent light absorption. *Appl. Phys. Lett.* **2018**, *113*, No. 022902.

(20) Pitcher, M. J.; Mandal, P.; Dyer, M. S.; Alaria, J.; Borisov, P.; Niu, H.; Claridge, J. B.; Rosseinsky, M. J. Tilt Engineering of Spontaneous Polarization and Magnetization Above 300 K in a Bulk Layered Perovskite. *Science* **2015**, *347*, 420−424.

(21) Bousquet, E.; Dawber, M.; Stucki, N.; Lichtensteiger, C.; Hermet, P.; Gariglio, S.; Triscone, J. M.; Ghosez, P. Improper Ferroelectricity in Perovskite Oxide Artificial Superlattices. *Nature* **2008**, *452*, 732−736.

(22) Zhu, T.; Cohen, T.; Gibbs, A. S.; Zhang, W.; Halasyamani, P. S.; Hayward, M. A.; Benedek, N. A. Theory and Neutrons Combine To Reveal a Family of Layered Perovskites without Inversion Symmetry. *Chem. Mater.* **2017**, *29*, 9489−9497.

(23) Snedden, A.; Knight, K. S.; Lightfoot, P. Structural distortions in the layered perovskites $CsANb_2O_7$ (A = Nd, Bi). *J. Solid State Chem.* **2003**, *173*, 309−313.

(24) Li, B. W.; Osada, M.; Ozawa, T. C.; Sasaki, T. $RbBiNb_2O_7$: A New Lead-Free High-T_c Ferroelectric. *Chem. Mater.* **2012**, *24*, 3111−3113.

(25) Chen, C.; Ning, H.; Lepadatu, S.; Cain, M.; Yan, H.; Reece, M. J. Ferroelectricity in Dion-Jacobson ABiNb(2)O(7) (A= Rb, Cs) compounds. *J. Mater. Chem. C* **2015**, *3*, 19−22.

(26) Goldschmidt, V. M. Die Gesetze der Krystallochemie. *Naturwissenschaften* **1926**, *14*, 477−485.

(27) Zhu, T.; Khalsa, G.; Havas, D. M.; Gibbs, A. S.; Zhang, W.; Shiv Halasyamani, P.; Benedek, N. A.; Hayward, M. A. Cation Exchange as a Mechanism to Engineer Polarity in Layered Perovskites. *Chem. Mater.* **2018**, *30*, 8915−8924.

(28) Mallick, S.; Gibbs, A. S.; Zhang, W.; Shiv Halasyamani, P.; Benedek, N. A.; Hayward, M. A. Polar Structures of $KNdNb_2O_7$ and $KNdTa_2O_7$. *Chem. Mater.* **2020**, *32*, 7965−7972.

(29) Mallick, S.; Khalsa, G.; Kaaret, J. Z.; Zhang, W.; Batuk, M.; Gibbs, A. S.; Hadermann, J.; Halasyamani, P. S.; Benedek, N. A.; Hayward, M. A. The influence of the $6s^2$ configuration of Bi^{3+} on the structures of $A'BiNb_2O_7$ (A' = Rb, Na, Li) layered perovskite oxides. *Dalton Trans.* **2021**, *50*, 15359−15369.

(30) Mallick, S.; Fortes, A. D.; Zhang, W.; Halasyamani, P. S.; Hayward, M. A. Switching between Proper and Hybrid-Improper Polar Structures via Cation Substitution in $A_2La(TaTi)O_7$ (A = Li, Na). *Chem. Mater.* **2021**, *33*, 2666−2672.

(31) Zhu, T.; Orlandi, F.; Manuel, P.; Gibbs, A. S.; Zhang, W.; Shiv Halasyamani, P.; Hayward, M. A. Directed synthesis of a hybrid improper magnetoelectric multiferroic material. *Nat. Commun.* **2021**, *12*, 4945.
(32) Guillou, F.; Thota, S.; Prellier, W.; Kumar, J.; Hardy, V. Magnetic transitions in Mn_3O_4 and an anomaly at 38 K in magnetization and specific heat. *Phys. Rev. B* **2011**, *83*, No. 094423.
(33) Jensen, G. B.; Nielsen, O. V. The Magnetic strucutre of Mn_3O_4 Hausmannite between 4.7K and Neel point, 41K. *J. Phys. C: Solid State Phys.* **1974**, *7*, 409−424.
(34) Chapon, L. C.; Manuel, P.; Radaelli, P. G.; Bensin, C.; Perrott, L.; Ansell, S.; Rhodes, N. J.; Raspino, D.; Duxbury, D.; Spill, E.; Norriss, J. Wish: The New Powder and Single Crystal Magnetic Diffractometer on the Second Target Station. *Neutron News* **2011**, *22*, 22−25.
(35) Coelho, A. A. TOPAS and TOPAS-Academic: an optimization program integrating computer algebra and crystallographic objects written in C++. *J. Appl. Crystallogr.* **2018**, *51*, 210−218.
(36) Ok, K. M.; Chi, E. O.; Halasyamani, P. S. Bulk characterization methods for non-centrosymmetric materials: second-harmonic generation, piezoelectricity, pyroelectricity, and ferroelectricity. *Chem. Soc. Rev.* **2006**, *35*, 710−717.
(37) Galven, C.; Mounier, D.; Bouchevreau, B.; Suard, E.; Bulou, A.; Crosnier-Lopez, M.-P.; Le Berre, F. Phase Transitions in the Ruddlesden-Popper Phase $Li_2CaTa_2O_7$: X-ray and Neutron Powder Thermodiffraction, TEM, Raman, and SHG Experiments. *Inorg. Chem.* **2016**, *55*, 2309−2323.
(38) Zhang, B. H.; Hu, Z. Z.; Chen, B. H.; Liu, X. Q.; Chen, X. M. Room-temperature ferroelectricity in A-site ordered Ruddlesden-Popper Li2CaTa2O7 ceramics. *J. Materiomics* **2020**, *6*, 593−599.
(39) Aleksandrov, K. S.; Bartolome, J. Octahedral Tilt Phases in Perovskite-like Crystals with Slabs Containing an Even Number of Octahedral Layers. *J. Phys.:Condens. Matter* **1994**, *6*, 8219−8235.
(40) Stokes, H. T.; Hatch, D. M., Campbell, B. J. iso.byu.edu, 2007.
(41) Campbell, B. J.; Stokes, H. T.; Tanner, D. E.; Hatch, D. M. ISODISPLACE: a web-based tool for exploring structural distortions. *J. Appl. Crystallogr.* **2006**, *39*, 607−614.

https://doi.org/10.1021/acs.chemmater.3c01850
Chem. Mater. 2023, 35, 7839−7846